Two-Dimensional Superlattices of Bi Nanoclusters Formed on a Au(111) Surface Using Porous Supramolecular Templates

Ran Zhang,[†] Guoqing Lyu,[†] Cheng Chen,[†] Tao Lin,[†] Jun Liu,[‡] Pei Nian Liu,*[,‡] and Nian Lin*[,†]

[†]Department of Physics, The Hong Kong University of Science and Technology, Clear Water Bay, Hong Kong, China and [‡]Shanghai Key Laboratory of Functional Materials Chemistry and Institute of Fine Chemicals, East China University of Science and Technology, Meilong Road 130, Shanghai 200237, China

ABSTRACT We used porous supramolecular structures as templates to make two-dimensional (2D) superlattices of Bi nanoclusters on a Au(111) surface. First, we applied on-surface self-assembly to prepare 2D porous supramolecular structures containing well-ordered nanopores. Then, we deposited Bi atoms on the surface. The Bi atoms were confined in the supramolecular pores and formed nanoclusters of a critical size that is defined by the pore size. These nanoclusters were arranged as a 2D superlattice dictated by the structure of the supramolecular templates. The nanocluster size and superlattice periodicity can be adjusted by appropriately designing the supramolecular structures. We further studied the formation mechanism of the nanoclusters. We found that Bi atoms could diffuse across the pore boundaries at room temperature and nucleated as clusters inside the pores. The clusters grew until they reached the critical size and became stable. We used kinetic Monte Carlo simulations to reproduce the experimental results and quantified the interpore diffusion barrier to be 0.65 eV.

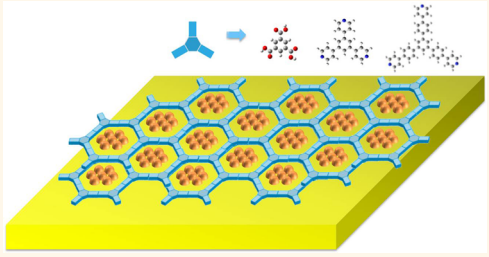

KEYWORDS: superlattice · supramolecular templates · Bi nanoclusters · scanning tunneling microscopy · kinetic Monte Carlo simulations

Metal nanoclusters have attracted much attention because of their unique size- and shape-dependent optical,[1,2] magnetic,[3−5] and catalytic properties.[6−8] Two-dimensional (2D) superlattices of metal nanoclusters are expected to possess tailor-made properties. Their optical and electronic properties depend greatly on their structure,[9] periodicity,[10] and intercluster spacing.[11−13] Various approaches for fabricating nanocluster superlattices have been reported.[14−19] For example, the dislocation patterns created by strain relieving can serve as templates for the formation of highly ordered 2D superlattices of nanoclusters on surfaces.[15] Graphene and boron nitride moiré patterns can play the same role, too.[16,17] Reconstructed 7 × 7 Si(111) surfaces were used to form same-sized nanoclusters of group III metals (Al, Ga, and In).[18−20] Recently, metal−organic pores were used to agglomerate Fe adatoms.[21,22] In this work, we use porous supramolecular networks as templates to make superlattices comprising uniform-sized bismuth (Bi) nanoclusters.

Bi is a main group element possessing unusual electronic properties, including low carrier density, small effective mass, and long mean free path.[23−30] Bulk Bi is a semimetal and exists in a wide range of functional materials such as magnets, superconductors, and thermoelectric and spintronic materials.[31−34] Due to size-induced quantum confinement effects, Bi nanoclusters exhibit novel electronic and chemical properties.[35−40] For example, Bi nanoclusters are the best catalysts for the solution−liquid−solid growth of diameter-controlled semiconductor quantum wires and rods. Recently, the discovery of Bi-based topological insulators has stimulated intensive interest in this material owing to its strong spin−orbital coupling effects.[41−43]

In this paper, we present an approach to making superlattices of Bi nanoclusters on a Au(111) surface. We used three molecules (see Scheme 1) to form supramolecular

* Address correspondence to phnlin@ust.hk, liupn@ecust.edu.cn.

Received for review June 17, 2015 and accepted August 4, 2015.

Published online August 04, 2015
10.1021/acsnano.5b03676

networks comprising 2D nanopores on a Au(111) surface. Molecules **1** at different surface coverage self-assembled into a series of networks stabilized by hydrogen bonds *via* their carboxyl groups.[44] These networks contained same-sized pores that were arranged in triangular lattices with different lattice constants. Molecules **2** and **3** coordinated with Cu atoms to form porous hexagonal networks with uniform 2D pores.[45,46] The Au(111) surface was covered with the porous supramolecular structures first, which was then dosed with Bi atoms. The Bi atoms formed stable nanoclusters in the pores. The nanoclusters were organized as 2D superlattices on the surface. The size of the Bi clusters is determined by the pore size, and the lattice constant of the superlattice is determined by the lattice constant of the supramolecular templates. As a result, the morphology and density of the superlattices can be adjusted by appropriately designing the supramolecular structures. We carried out annealing experiments to investigate the template effects and propose a mechanism to understand these effects. Based on the proposed mechanism, we reproduced the experimental results using kinetic Monte Carlo (kMC) simulations and quantitatively determined the energetics of the template effects.

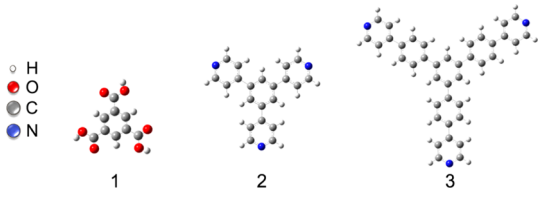

Scheme 1. Chemical structures of the three molecules used in this study: trimesic acid (TMA) (1), 1,3,5-tris(pyridyl)benzene (2), and 1,3,5-tris[4-(pyridin-4-yl)phenyl]benzene (3).

RESULTS AND DISCUSSION

At a coverage of 0.3 ML (1 ML refers to closely packed molecules on the surface), molecule **1** formed a homogeneous honeycomb network structure, denoted as the TMA-**1** phase hereafter.[44] This phase contains hexagonal-shaped pores with an inner diameter of 1.20 nm. Note that the inner diameter is estimated based on the structural model, taking into account the van der Waals radius of the atoms. The pores are arranged in a triangular lattice with a pore-to-pore distance of 1.65 nm. Figure 1a shows that, after depositing ~0.17 ML of Bi on this sample, the network structure remained intact, while bright dots showed up in 26% of the pores. The dots appeared to be very uniform in shape, height, and size. Their apparent diameter is ~1.24 nm and apparent height is ~0.26 nm relative to the Au(111) surface. After more Bi was added to reach 0.33 ML, bright dots appeared in 97% of the pores, as can be seen in Figure 1b, suggesting that the bright dots were actually clusters of Bi atoms. We successively increased the Bi dosage and statistically analyzed the population of Bi clusters to estimate the number of Bi atoms in a cluster (see Supporting Information for analysis details). The number of Bi

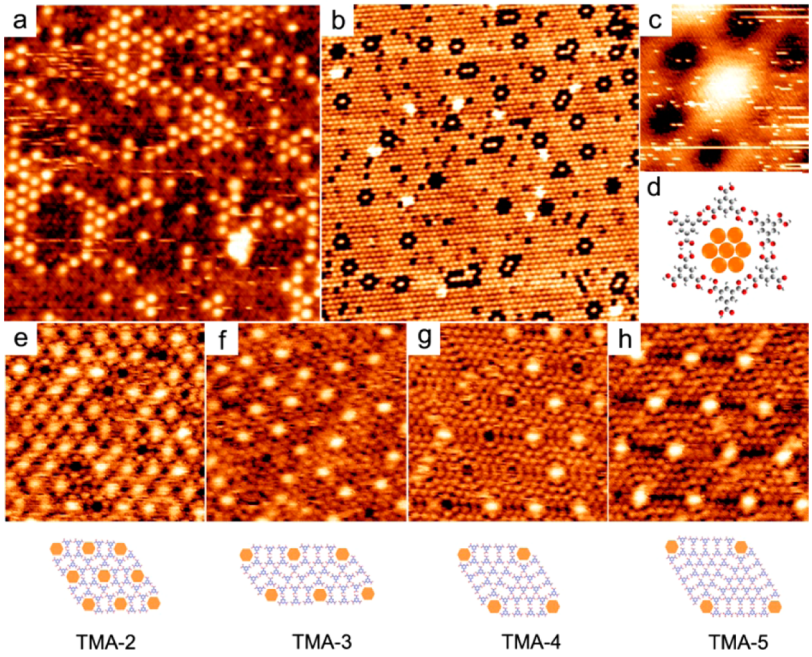

Figure 1. STM topographs showing (a) Bi nanoclusters (bright dots) formed in the TMA-1 template (40 × 40 nm^2) at 0.17 ML of Bi; (b) Bi nanocluster superlattice formed in the TMA-1 template (90 × 90 nm^2) at 0.33 ML of Bi; and (c) magnified view of a Bi nanocluster confined in a pore (4.5 × 4.5 nm^2). (d) Tentative model showing a Bi nanocluster comprising seven closely packed Bi atoms (orange spheres) with an atom spacing of 0.33 nm. (e–h) Top row: STM topographs showing Bi nanocluster superlattices formed in the TMA-2, TMA-3, TMA-4, and TMA-5 templates (20 × 20 nm^2). Bottom row: models of the superlattices where the orange dots represent seven-atom Bi nanoclusters.

atoms in a nanocluster was determined to be seven. A model showing seven Bi atoms forming a closely packed cluster in a pore is shown in Figure 1d, where the interatomic spacing is 0.33 nm, which is the same as the lattice constant of Bi bulk crystals. Figure 1c is a scanning tunneling microscopy (STM) topograph showing a nanocluster completely filling a pore, whereas the neighboring pores are empty. This observation suggests that (1) the Bi atoms can diffuse across the boundaries of the 2D supramolecular pores and (2) the Bi cluster that completely fills a pore is stable.

A series of other network phases, denoted as TMA-*n* ($n = 2-5$), formed when we increased the dosage of molecule **1** on the surface above 0.6 ML.[44] These structures contain the same hexagonal pores as the TMA-**1** phase. These pores are arranged in triangular lattices, but the pore-to-pore distances increase as *n* grows. Table 1 lists the lattice constants of the five structures observed in our study. After being deposited on these templates, the Bi atoms formed nanoclusters of the same size in the pores as those formed in the TMA-**1** template. Figure 1e–h shows that the Bi nanoclusters are organized in superlattices whose periodicity is defined by the TMA-*n* templates. The models of the four superlattices are displayed below the STM topographs.

Molecule **2** and molecule **3** coordinated with Cu atoms to form porous metal–organic networks on Au(111), denoted as **2**-Cu and **3**-Cu templates, respectively. The **2**-Cu (**3**-Cu) template contains pores with an inner diameter of 1.9 nm (3.4 nm) that are arranged in a triangular lattice with a 2.6 nm (4.0 nm) lattice constant. Figure 2a shows that, after depositing 0.28 ML of Bi on the **2**-Cu template, uniform bright dots appeared in the pores. The number of the dots increased linearly with the dosage of Bi (see Supporting Information), thus these bright dots can also be attributed to Bi clusters. At a Bi dosage of 0.34 ML, 55% of pores were filled with the Bi nanoclusters. Figure 2b is a high-resolution image showing a Bi nanocluster completely filling a hexagonal pore of the **2**-Cu template. A model is drawn in Figure 2c, showing that the maximum number of Bi atoms in a nanocluster was 19 when Bi atoms were closely packed at an interatomic spacing of 0.33 nm. Besides the bright clusters, Figure 2b also resolved some faint features in the pores. These features very often underwent changes or moved during scanning (see detailed discussion below). We attribute them to smaller Bi clusters or moving Bi adatoms. Figure 2d shows Bi nanoclusters formed by depositing 0.67 ML of Bi on the **3**-Cu template. In this sample, 45% of the pores were filled with the Bi nanoclusters. In contrast to Figure 1 and Figure 2a, the nanoclusters formed in this template are not uniform and do not arrange in a perfect triangular lattice. Figure 2e is a STM topography showing a pore filled with a nanocluster. Figure 2f shows a model of the Bi nanocluster formed in a hexagonal pore of the **3**-Cu template. The 3.4 nm inner diameter of the pores allowed a maximum of 61 closely packed Bi atoms with an interatomic spacing of 0.33 nm. Similarly, the faint features in the surrounding pores are attributed to smaller Bi clusters or moving Bi adatoms.

We quantitatively analyzed the cluster size distribution of the Bi nanoclusters formed in the three types of templates. The results are plotted in Figure 3. The nanoclusters formed in the TMA templates display a very narrow size distribution (black): 87% of the clusters fall within a range of 1.3 ± 0.2 nm^2, which is slightly larger than the van der Waals pore size of 1.1 nm^2 (the van der Waals pore size is calculated according to the inner diameter). The size distribution clearly indicates

TABLE 1. Lattice Constant and Bi Nanocluster Density of Five Bi Nanocluster Superlattices Formed in the Template TMA-*n* ($n = 1-5$)

template	lattice constant (nm)	density of Bi nanoclusters (per 100 nm^2)
TMA-**1**	1.65	42.4
TMA-**2**	2.55	17.8
TMA-**3**	3.55	9.16
TMA-**4**	4.38	6.02
TMA-**5**	5.30	4.11

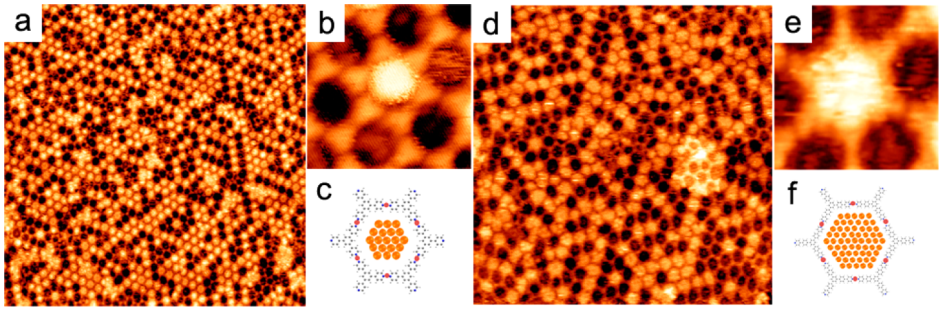

Figure 2. (a) STM topograph showing a Bi cluster superlattice formed after depositing 0.28 ML of Bi on the 2-Cu template (90×90 nm^2). (b) High-resolution STM topograph showing the hexagonal pore and a Bi cluster (7×7 nm^2). (c) Tentative model showing 19 Bi atoms closely packed in the pore. (d) STM topograph showing a Bi cluster superlattice formed after depositing 0.67 ML of Bi on the 3-Cu template (90×90 nm^2). (e) High-resolution STM topograph showing the larger hexagonal pore and a Bi cluster (9×9 nm^2). (f) Tentative model showing 61 Bi atoms closely packed in the pore.

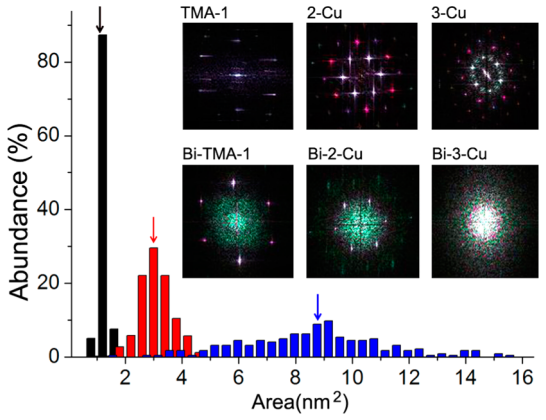

Figure 3. Size distribution of Bi nanoclusters formed in TMA-1 (black), 2-Cu (red), and 3-Cu (blue) templates. The arrows mark the van der Waals pore size of the three templates. Inset: Fourier transformation of the TMA-1, 2-Cu, and 3-Cu templates without (top row) and with (bottom row) Bi nanocluster superlattices.

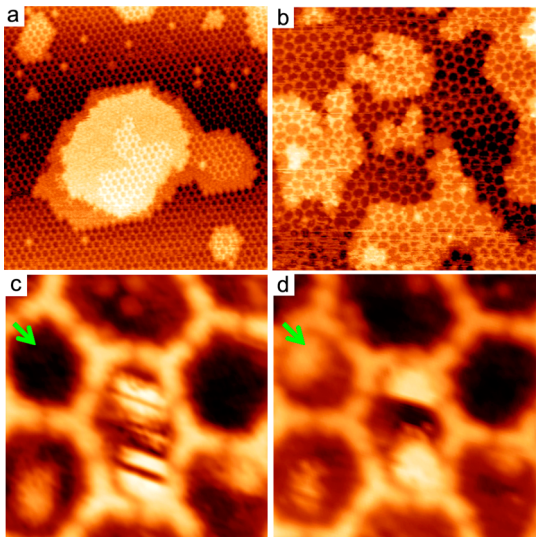

Figure 4. Two-dimensional Bi islands formed in the (a) 2-Cu template (90 × 90 nm^2) and (b) 3-Cu template (100 × 100 nm^2) after annealing the sample, as shown in Figure 2a,d, respectively, at 100 °C. (c,d) STM topographs scanning the same area of the 3-Cu template acquired 5 min apart (14 × 14 nm^2).

that Bi nanoclusters with the uniform size can be made using TMA templates. The size distribution is broader in the **2**-Cu template (red): 30% of the clusters fall within a range of 3.0 ± 0.2 nm^2, in line with the van der Waals pore size of 3.0 nm^2 (marked by the red arrow). In the **3**-Cu template, the cluster size distribution is even broader, ranging from 2 to 16 nm^2. Only about 10% of the clusters fall in the range of the van der Waals pore size of 9.0 ± 0.2 nm^2 (marked by the blue arrow). In Figure 2d, one can see that the supramolecular templates of **3**-Cu were partially distorted after filling with the Bi nanoclusters. Some parts of the template contained pentagonal and heptagonal pores that are smaller or bigger than the perfect hexagonal pores. This feature explains the broad cluster size in the **3**-Cu templates. To reveal the structural ordering, we present in the inset in Figure 3 the Fourier transformation of the three superlattices and compare them with the Fourier transformation of the empty supramolecular templates. The three empty templates all showed six sharp dots, reflecting their hexagonal structure. The superlattice formed in the TMA-**1** template displayed six dots that were almost as sharp as those of the empty TMA-**1** template, revealing a highly regular superlattice structure. The superlattice formed in the **2**-Cu template also showed six dots, but the dots are not as sharp as the empty **2**-Cu template. The nanoclusters formed in the **3**-Cu template did not show any recognizable dots in the Fourier transformation, corroborating the disordered distributed nanoclusters observed in Figure 2d.

We performed annealing experiments to test the thermal stability of the Bi nanocluster superlattices. The superlattices formed in all three templates behaved similarly in response to thermal annealing. At 100 °C, the Bi nanoclusters in the pores gradually disappeared. In other words, more and more of the pores that were filled with the nanoclusters became empty. In the meantime, compact 2D Bi islands formed and grew larger. Figure 4a,b presents STM topographs of the samples shown in Figure 2a,d, respectively, after annealing at 100 °C. In both samples, almost all pores were empty and large Bi 2D islands appeared. The annealing experiments indicate that the Bi nanocluster superlattices were not thermodynamically stable structures but were kinetically controlled. The Bi atoms released from the pores nucleated as 2D islands at the domain boundaries of the template structures or at step edges of the Au surface. Expansion of the Bi 2D islands took up the surface area that was formerly occupied by the supramolecular templates and disintegrates the latter. Interestingly, on top of the Bi islands, Cu and molecule **2** or **3** assembled into the same hexagonal network structures.

Next, we discuss the underlying formation mechanism of the Bi nanoclusters. At submonolayer dosage, Bi atoms are highly mobile on a bare Au(111) surface at room temperature. As deposited on the surface that is covered by the templates, the Bi atoms may be able to diffuse across the pore boundaries without destroying the template structure. Figure 4c,d shows two STM images of the **3**-Cu template acquired 5 min apart. They resolve the dynamics of Bi atoms. A close inspection of the two images reveals that (1) there are three faint dots inside the top-middle pore in the first image but none in the second image, (2) the bright cluster in the central pore has straight and sharp edges that are parallel to the scan direction, and (3) the pore marked by the green arrow is empty in the first image but contains a cluster in the second image: (1) indicates inside-pore diffusion of Bi atoms; (2) can be explained by the inside-pore diffusion of Bi clusters because the

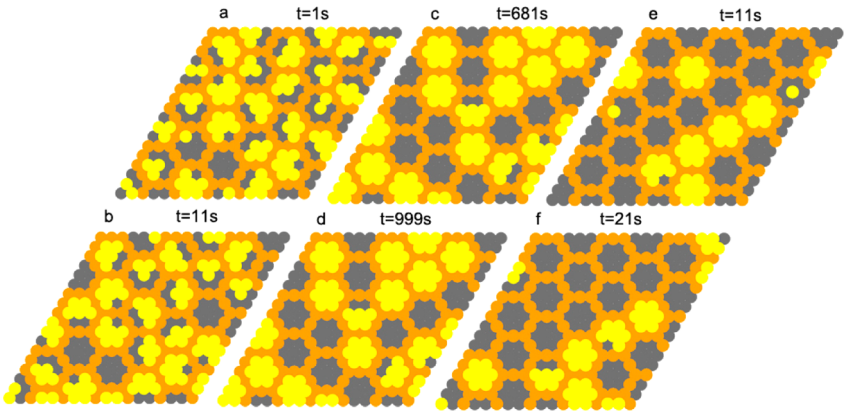

Figure 5. Kinetic Monte Carlo simulation of Bi clusters confined in templates with the diffusion energy barrier of the molecular potential wells being 0.65 eV: (a) t = 1 s, T = 300 K; (b) t = 11 s, T = 300 K; (c) t = 681 s, T = 300 K; (d) t = 999 s, T = 300 K; (e) t = 11 s, T = 353 K; (f) t = 21 s, T = 353 K.

straight and sharp edges imply that the cluster had moved away during scanning; (3) provides direct evidence for the interpore diffusion of Bi atoms.

On the basis of these findings, we propose a mechanism for the growth of the nanoclusters in the templates. Upon deposition, the Bi atoms randomly land on the surface. Experimentally, we observed that the Bi atoms do not form 2D islands on the clean surface, indicating that the Bi−Bi bond is weak and the diffuse barrier of Bi on the clean surface is low. When the Bi atoms diffuse across a molecule, they experience a larger barrier. Thus, the interpore diffusion barrier is higher. Due to the weak Bi−Bi bond and low diffusion barrier on the clean surface, the small clusters that formed inside the pores easily disintegrate into single atoms if they do not border the pore boundaries. However, when a cluster completely fills a pore, defined as the critical size, each edge atom is bound by three Bi−Bi bonds on one side and faces the interpore diffusion barrier on the other side. These effects trap the edge atoms and thus stabilize the cluster. At 100 °C, the templates are still stable,[47] while the thermal energy is high enough for the edge atoms to escape and diffuse across the pore boundary. As a result, the clusters that have reached critical size will dissolve at 100 °C.

We used kMC method to simulate the nanocluster formation in the pores. Three energy terms were taken into account: the binding energy (E_b) between two nearest-neighboring Bi atoms, the diffusion barrier (E_d) of the Bi adatom on the clean substrate, and the interpore diffusion barrier (E_i). We ran the simulations with multiple sets of the three energetic parameters to reproduce the following experimental observations: (1) Bi atoms do no form stable islands on the clean surface at 300 K; (2) Bi atoms can diffuse across the template boundaries at 300 K; (3) Bi clusters of the critical size in the pores are stable at 300 K but dissolve at 350 K. We found that the values of E_b = 0.10 eV, E_d = 0.30 eV, and E_i = 0.65 eV satisfactorily reproduced all experimental data. Figure 5a−d displays the simulated structures at 300 K. Initially (Figure 5a), the Bi atoms were randomly distributed in the pores and no single pore was completely filled. Figure 5b shows that the structures underwent many changes within a short period of just 10 s. Comparison of the two images features interpore diffusion of individual atoms, dissociation, displacement, and rotation of clusters inside the pores. All of these changes are consistent with the experimental observations presented in Figure 4c,d. Figure 5c shows that, after 680 s, 12 pores were completed filled with critical-size clusters, each containing seven Bi atoms. These clusters were very stable and remained unchanged at 999 s (Figure 5d), while the unfilled clusters underwent frequent structural changes. The formation and stability of the critical-size clusters in the simulations are in good agreement with the experimental data. We also ran the simulation at 353 K. At t = 11 s, six pores were completely filled with critical-size clusters (Figure 5e). After 10 s, one-half of these clusters had dissolved, indicating that the critical-size clusters were unstable at 353 K. This behavior reproduces the structural changes observed in the annealing experiments.

CONCLUSION

We have demonstrated the growth of Bi nanocluster superlattices on a Au(111) surface using porous supramolecular templates. The nanocluster size and superlattice periodicity were dictated by the template structure, namely, the pore size and pore periodicity. We propose a formation mechanism involving effective interpore diffusion for free adatoms and inhibited interpore diffusion for the edge atoms in the critical-size clusters. The kMC simulations reproduced the experimental findings at the interpore diffusion barrier of 0.65 eV. This value is much larger than the diffusion barrier of 0.30 eV of Bi adatoms on a clean surface but allows efficient interpore diffusion at room temperature. The new strategy could potentially enable the fabrication of 2D nanocluster arrays on surfaces using

supramolecular structures as the template. Finally, we specify an application of the Bi cluster superlattices. It was demonstrated that periodic potential provided by molecules with a triangular lattice on a metal surface can generate massless Dirac fermions, whose characteristics are tunable by changing the lattice parameters, known as artificial graphene.[48−50] Hughes *et al.* argued that the 2D quantum spin-Hall insulator can be realized in such artificial graphene systems if a strong spin−orbit effect is introduced.[51] Owing to the large spin−orbital coupling effect in Bi, we expect that the Bi cluster superlattice formed on Au(111) may be a promising candidate for realizing the artificial 2D quantum spin-Hall insulator.

METHODS

All samples were prepared in an ultrahigh vacuum system with a base pressure of 3×10^{-10} mbar. A single-crystalline Au(111) substrate was cleaned by repeatedly performing Ar^+ sputtering and annealing at 620 °C. Molecules **1**, **2**, and **3** were deposited onto the Au(111) surface at room temperature. The evaporation temperatures were 210, 225, and 390 °C for molecules **1**, **2**, and **3** respectively. After deposition, the sample of molecule **1** was annealed to 160 °C and formed networks. For molecules **2** or **3**, the Cu-coordinated networks formed after depositing Cu on the sample and annealing to 220 °C. The Au(111) surface was dosed with Bi atoms using a home-built electron-beam evaporator. The evaporation speed was ~0.17 ML/min. All data were acquired by STM at room temperature in a constant-current mode. All STM data were imaged with $U = -1.1$ V and $I = 0.26$ nA. The data were processed using the WSxM software.[52]

The kinetic Monte Carlo (KMC) simulations were performed on a hexagonal lattice with periodic boundary conditions using a previously described algorithm.[53] A honeycomb potential well was placed on the lattice. A single Bi atom occupied a lattice site. Fifty percent of the free sites were occupied by Bi atoms in the simulations. An individual Bi atom can hop to the nearest-neighbor site within a pore or to a site in the nearest-neighbor pore. The energy barriers to these two hopping events are defined by E_d and E_i. Two nearest-neighbor Bi atoms are bound by an attractive bond (E_b).

Conflict of Interest: The authors declare no competing financial interest.

Supporting Information Available: The Supporting Information is available free of charge on the ACS Publications website at DOI: 10.1021/acsnano.5b03676.

Statistical analysis of the number of Bi atoms in the nanoclusters, and Bi nanoclusters formed in **2**-Cu and **3**-Cu templates with successively increased Bi dosage (PDF)

Acknowledgment. This work is financially supported by Hong Kong RGC 16303514 and NSFC (Project Nos. 21421004 and 21190033).

REFERENCES AND NOTES

1. El-Sayed, M. A. Some Interesting Properties of Metals Confined in Time and Nanometer Space of Different Shapes. *Acc. Chem. Res.* **2001**, *34*, 257–264.
2. Jin, R.; Cao, Y. C.; Hao, E.; Metraux, G. S.; Schatz, G. C.; Mirkin, C. A. Controlling Anisotropic Nanoparticle Growth through Plasmon Excitation. *Nature* **2003**, *425*, 487–490.
3. Sun, S.; Murry, C. B.; Weller, D.; Folks, L.; Moser, A. Monodisperse FePt Nanoparticles and Ferromagnetic FePt Nanocrystal Superlattices. *Science* **2000**, *287*, 1989–1992.
4. Puntes, V. F.; Krishnan, K. M.; Alivisatos, A. P. Colloidal Nanocrystal Shape and Size Control: The Case of Cobalt. *Science* **2001**, *291*, 2115–2117.
5. Dumestre, F.; Chaudret, B.; Amiens, C.; Renaud, P.; Fejes, P. Superlattices of Iron Nanocubes Synthesized from Fe[N(SiMe$_3$)$_2$]$_2$. *Science* **2004**, *303*, 821–823.
6. Narayanan, R.; El-Sayed, M. A. Catalysis with Transition Metal Nanoparticles in Colloidal Solution: Nanoparticle Shape Dependence and Stability. *J. Phys. Chem. B* **2005**, *109*, 12663–12676.
7. Habas, S. E.; Lee, H.; Radmilovic, V.; Somorjai, G. A.; Yang, P. Shaping Binary Metal Nanocrystals through Epitaxial Seeded Growth. *Nat. Mater.* **2007**, *6*, 692–697.
8. Xiong, Y.; Wiley, B. J.; Xia, Y. Nanocrystals with Unconventional Shapes—A Class of Promising Catalysts. *Angew. Chem., Int. Ed.* **2007**, *46*, 7157–7159.
9. Kim, S.-H.; Medeiros-Ribeiro, G.; Ohlberg, D. A. A.; Williams, R. S.; Heath, J. R. Individual and Collective Electronic Properties of Ag Nanocrystals. *J. Phys. Chem. B* **1999**, *103*, 10341–10347.
10. Kim, B.; Tripp, S. L.; Wei, A. Self-Organization of Large Gold Nanoparticle Arrays. *J. Am. Chem. Soc.* **2001**, *123*, 7955–7956.
11. Collier, C. P.; Saykally, R. J.; Shiang, J. J.; Henrichs, S. E.; Heath, J. R. Reversible Tuning of Silver Quantum Dot Monolayers through the Metal-Insulator Transition. *Science* **1997**, *277*, 1978–1981.
12. Beverly, K. C.; Sampaio, J. F.; Heath, J. R. Effects of Size Dispersion Disorder on the Charge Transport in Self-Assembled 2-D Ag Nanoparticle Arrays. *J. Phys. Chem. B* **2002**, *106*, 2131–2135.
13. Frankamp, B. L.; Boal, A. K.; Rotello, V. M. Controlled Interparticle Spacing through Self-Assembly of Au Nanoparticles and Poly(amidoamine) Dendrimers. *J. Am. Chem. Soc.* **2002**, *124*, 15146–15147.
14. Lin, X. M.; Jaeger, H. M.; Sorensen, C. M.; Klabunde, K. J. Formation of Long-Range-Ordered Nanocrystal Superlattices on Silicon Nitride Substrates. *J. Phys. Chem. B* **2001**, *105*, 3353–3357.
15. Brune, H.; Giovannini, M.; Bromann, K.; Kern, K. Self-Organized Growth of Nanostructure Arrays on Strain-Relief Patterns. *Nature* **1998**, *394*, 451–453.
16. N'Diaye, A. T.; Gerber, T.; Busse, C.; Mysliveček, J.; Coraux, J.; Michely, T. A Versatile Fabrication Method for Cluster Superlattices. *New J. Phys.* **2009**, *11*, 1–19.
17. Patterson, M. C.; Habenicht, B. F.; Kurtz, R. L.; Liu, L.; Xu, Y.; Sprunger, P. T. Formation and Stability of Dense Arrays of Au Nanoclusters on Hexagonal Boron Nitride/Rh(111). *Phys. Rev. B: Condens. Matter Mater. Phys.* **2014**, *89*, 205423.
18. Kotlyar, V. G.; Zotov, A. V.; Saranin, A. A.; Kasyanova, T. V.; Cherevik, M. A.; Pisarenko, I. V.; Lifshits, V. G. Formation of the Ordered Array of Al Magic Clusters on Si(111) 7×7. *Phys. Rev. B: Condens. Matter Mater. Phys.* **2002**, *66*, 165401.
19. Li, J.-L.; Jia, J.-F.; Liang, X.-J.; Liu, X.; Wang, J.-Z.; Xue, Q.-K.; Li, Z.-Q.; Tse, J. S.; Zhang, Z.; Zhang, S. B. Spontaneous Assembly of Perfectly Ordered Identical-Size Nanocluster Arrays. *Phys. Rev. Lett.* **2002**, *88*, 066101.
20. Lai, M. Y.; Wang, Y. L. Self-Organized Two-Dimensional Lattice of Magic Clusters. *Phys. Rev. B: Condens. Matter Mater. Phys.* **2001**, *64*, 241404.
21. Pivetta, M.; Pacchioni, G. E.; Schlickum, U.; Barth, J. V.; Brune, H. Formation of Fe Cluster Superlattice in a Metal-Organic Quantum-Box Network. *Phys. Rev. Lett.* **2013**, *110*, 086102.
22. Decker, R.; Schlickum, U.; Klappenberger, F.; Zoppellaro, G.; Klyatskaya, S.; Ruben, M.; Barth, J. V.; Brune, H. Using Metal-Organic Templates to Steer the Growth of Fe and Co Nanoclusters. *Appl. Phys. Lett.* **2008**, *93*, 243102.
23. Ashcroft, N. W.; Mermin, D. N. *Solid State Physics*, 1st ed.; Thomson Learning: Toronto, 1976.
24. Yang, F. Y.; Liu, K.; Hong, K.; Reich, D. H.; Searson, P. C.; Chien, C. L. Large Magnetoresistance of Electrodeposited

Single-Crystal Bismuth Thin Films. *Science* **1999**, *284*, 1335–1337.
25. Behnia, K.; Balicas, L.; Kopelevich, Y. Signatures of Electron Fractionalization in Ultraquantum Bismuth. *Science* **2007**, *317*, 1729–1731.
26. Li, L.; Checkelsky, J. G.; Hor, Y. S.; Uher, C.; Hebard, A. F.; Cava, R. J.; Ong, N. P. Phase Transitions of Dirac Electrons in Bismuth. *Science* **2008**, *321*, 547–550.
27. Liu, K.; Chien, C. L. Finite-Size Effects in Bismuth Nanowires. *Phys. Rev. B: Condens. Matter Mater. Phys.* **1998**, *58*, R14681.
28. Heremans, J.; Thrush, C. M.; Zhang, Z.; Sun, X.; Dresselhaus, M. S.; Ying, J. Y.; Morelli, D. T. Magnetoresistance of Bismuth Nanowire Arrays: A Possible Transition from One-Dimensional to Three-Dimensional Localization. *Phys. Rev. B: Condens. Matter Mater. Phys.* **1998**, *58*, R10091.
29. Heremans, J.; Thrush, C. M.; Lin, Y.-M.; Cronin, S.; Zhang, Z.; Dresselhaus, M. S.; Mansfield, J. F. Bismuth Nanowire Arrays: Synthesis and Galvanomagnetic Properties. *Phys. Rev. B: Condens. Matter Mater. Phys.* **2000**, *61*, 2921–2930.
30. Lin, Y.-M.; Sun, X.; Dresselhaus, M. S. Theoretical Investigation of Thermoelectric Transport Properties of Cylindrical Bi Nanowires. *Phys. Rev. B: Condens. Matter Mater. Phys.* **2000**, *62*, 4610–4623.
31. Hansen, P.; Witter, K.; Tolksdorf, W. Magnetic and Magneto-Optic Properties of Lead- and Bismuth-Substituted Yttrium Iron Garnet Films. *Phys. Rev. B: Condens. Matter Mater. Phys.* **1983**, *27*, 6608–6625.
32. Eisaki, H.; Kaneko, N.; Feng, D. L.; Damascelli, A.; Mang, P. K.; Shen, K. M.; Shen, Z.-X.; Greven, M. Effect of Chemical Inhomogeneity in Bismuth-Based Copper Oxide Superconductors. *Phys. Rev. B: Condens. Matter Mater. Phys.* **2004**, *69*, 064512.
33. Heremans, J.; Thrush, C. M. Thermoelectric Power of Bismuth Nanowires. *Phys. Rev. B: Condens. Matter Mater. Phys.* **1999**, *59*, 12579.
34. Catalan, G.; Scott, J. F. Physics and Applications of Bismuth Ferrite. *Adv. Mater.* **2009**, *21*, 2463–2485.
35. Dresselhaus, M. S.; Lin, Y. M.; Rabin, O.; Jorio, A.; Souza Filho, A. G.; Pimenta, M. A.; Saito, R.; Samsonidze, G.; Dresselhaus, G. Nanowires and Nanotubes. *Mater. Sci. Eng., C* **2003**, *23*, 129–140.
36. Hicks, L. D.; Dresselhaus, M. S. Thermoelectric Figure of Merit of a One-Dimensional Conductor. *Phys. Rev. B: Condens. Matter Mater. Phys.* **1993**, *47*, 16631–16634.
37. Heremans, J. P.; Thrush, C. M.; Morelli, D. T.; Wu, M.-C. Thermoelectric Power of Bismuth Nanocomposites. *Phys. Rev. Lett.* **2002**, *88*, 216801.
38. Yu, H.; Li, J.; Loomis, R. A.; Gibbons, P. C.; Wang, L.-W.; Buhro, W. E. Cadmium Selenide Quantum Wires and the Transition from 3D to 2D Confinement. *J. Am. Chem. Soc.* **2003**, *125*, 16168–16169.
39. Wang, F.; Dong, A.; Sun, J.; Tang, R.; Yu, H.; Buhro, W. E. Solution-Liquid-Solid Growth of Semiconductor Nanowires. *Inorg. Chem.* **2006**, *45*, 7511–7521.
40. Grebinski, J. W.; Hull, K. L.; Zhang, J.; Kosel, T. H.; Kuno, M. Solution-Based Straight and Branched CdSe Nanowires. *Chem. Mater.* **2004**, *16*, 5260–5272.
41. Hofmann, Ph. The Surfaces of Bismuth: Structural and Electronic Properties. *Prog. Surf. Sci.* **2006**, *81*, 191–245.
42. Hasan, M. Z.; Kane, C. L. Colloquium: Topological Insulators. *Rev. Mod. Phys.* **2010**, *82*, 3045–3067.
43. Qi, X.-L.; Zhang, S.-C. Topological Insulator and Superconductor. *Rev. Mod. Phys.* **2011**, *83*, 1057–1110.
44. Ye, Y.; Sun, W.; Wang, Y.; Shao, X.; Xu, X.; Cheng, F.; Li, J.; Wu, K. A Unified Model: Self-Assembly of Trimesic Acid on Gold. *J. Phys. Chem. C* **2007**, *111*, 10138–10141.
45. Liu, J.; Lin, T.; Shi, Z.; Xia, F.; Dong, L.; Liu, P. N.; Lin, N. Structural Transformation of Two-Dimensional Metal Organic Coordination Networks Driven by Intrinsic In-Plane Compression. *J. Am. Chem. Soc.* **2011**, *133*, 18760–18766.
46. Wang, S.; Wang, W.; Tan, L. Z.; Li, X. G.; Shi, Z.; Kuang, G.; Liu, P. N.; Louie, S. G.; Lin, N. Tuning Two-Dimensional Band Structure of Cu(111) Surface-State Electrons that Interplay with Artificial Supramolecular Architectures. *Phys. Rev. B: Condens. Matter Mater. Phys.* **2013**, *88*, 245430.
47. Shi, Z.; Liu, J.; Lin, T.; Xia, F.; Liu, P. N.; Lin, N. Thermodynamics and Selectivity of Two-Dimensional Metallo-supramolecular Self-Assembly Resolved at Molecular Scale. *J. Am. Chem. Soc.* **2011**, *133*, 6150–6153.
48. Park, C.-H.; Louie, S. G. Making Massless Dirac Fermions from a Patterned Two-Dimensional Electron Gas. *Nano Lett.* **2009**, *9*, 1793–1797.
49. Gomes, K. K.; Mar, M.; Ko, W.; Guinea, F.; Manoharan, H. C. Designer Dirac Fermions and Topological Phases in Molecular Graphene. *Nature* **2012**, *483*, 306–310.
50. Wang, S.; Liang, Z. T.; Wang, W.; Louie, S. G.; Lin, N. Manipulation and Characterization of Aperiodical Graphene Structures Created in a Two-Dimensional Electron Gas. *Phys. Rev. Lett.* **2014**, *113*, 196803.
51. Ghaemi, P.; Gopalakrishnan, S.; Hughes, T. L. Designer Quantum Spin Hall Phase Transition in Molecular Graphene. *Phys. Rev. B: Condens. Matter Mater. Phys.* **2012**, *86*, 201406(R).
52. Horcas, I.; Fernández, R.; Gómez-Rodríguez, J. M.; Colchero, J.; Gómez-Herrero, J.; Baro, A. M. WSXM: A Software for Scanning Probe Microscopy and a Tool for Nanotechnology. *Rev. Sci. Instrum.* **2007**, *78*, 013705.
53. Li, Y.; Lin, N. Combined Scanning Tunneling Microscopy and Kinetic Monte Carlo Study on Kinetics of Cu-Coordinated Pyridyl-Porphyrin Supramolecular Self-Assembly on a Au(111) Surface. *Phys. Rev. B: Condens. Matter Mater. Phys.* **2011**, *84*, 125418.